P6.15

VORTEX-LINES AND AIRFLOW STRUCTURE NEAR A TORNADO-LIKE VORTEX IN A SIMULATED MINI-SUPERCELL

Akira NODA*and Hiroshi NIINO
Dynamic Marine Meteorology Group, Division of Physical Oceanography
Ocean Research Institute, University of Tokyo

1. INTRODUCTION

Since their conceptual model was proposed by Browning (1964), supercell thunderstorms have been extensively studied. It is now widely recognized that supercell thunderstorms have a wide spectrum. Typical supercell storms that fit in Browning's conceptual model are now called 'classic supercells'. At the lowest end of the spectrum, there exist a class of storms called 'mini-supercell'. They are known to occur often in a typhoon/hurricane environment. They have small dimensions both in the horizontal and vertical directions, They not only possess a hook-shaped rain water pattern, a vault structure and a mesocyclone (hereafter MC), but also occasionally spawn intense tornadoes (McCaul and Weisman, 1996; Suzuki et al., 2000). They are also known to have a very similar airflow structure to Browning's conceptual model (Noda, 2000). The environment for mini-supercells is characterized by relatively small CAPE and strong low-level vertical wind shear (Novlan and Gray, 1974; McCaul, 1991)

During the last two decades, our understanding of the supercells have been considerably advanced. At the earlier stage of their evolution, the supercells split into northern and southern storms. After several tens minutes, the southern storm selectively develops. As a result, the supercell appears to travel rightward relative to the mean wind. Rotunno and Klemp (1982) has shown that this right-moving behavior is a result of an interaction between the updraft and the environmental vertical wind shear: At the mid-level, low pressure appears in the southern side of the updraft, while high pressure in the north side. Due to a vertical pressure gradient force (PGF), the updraft of the southern storm is enhanced, while that of the northern storm is weakened. Around this time, a storm-scale downdraft begins to develop from the mid-level, wrap around the main updraft and descends cyclonically (Burgess et al., 1977; Klemp et al., 1981). Klemp and Rotunno (1983) showed that there appears another smaller-scale downdraft driven by dynamic pressure force relating to the intense low-level rotation in its tornadic phase. They named it an occlusion downdraft.

Although the dynamics of the updraft has been extensively studied, that of the storm-scale downdraft originating from the mid-level seems to have paid relatively little attention. It has been considered simply to be a compensation flow for the updraft or to be driven by a negative buoyancy owing to loading of hydrometeors and their evaporative cooling. However, recent studies on the origin of vorticity in the low-level MC (e.g., Niino and Noda, 2000) show that the mid-level horizontal vorticity contributes significantly to the vertical vorticity in the MC, and the downdraft plays an important role for conveying the vorticity to the low-level. Thus, in order to understand the vorticity dynamics in a supercell, the dynamics of the storm-scale downdraft needs to be clarified.

In this study, we shall examine the dynamics the downdraft using the result of the high-resolution simulation of a tornadic mini-supercell which occurred over Kanto plain, Japan on 19 September 1990. The simulated mini-supercell spawned a tornado-like vortex (hereafter TV, which is referred to the vertical vorticity exceeding 0.1 s^{-1}). Its vorticity dynamics is also studied.

2. METHODOLOGY AND MODEL INITIALIZATION

The numerical model used for the present simulation is the parallel version of ARPS Ver. 4.5.1 (Xue et al., 1995). The spatial resolution in the horizontal direction is homogeneous and is 150 m. That in the vertical direction increases from 50 m near the ground to 550 m near the top of the calculation domain. Free-slip rigid wall and adiabatic boundary conditions are assumed at the vertical boundaries. Radiation conditions are used at the lateral open boundaries. A Rayleigh damping of an e-folding time of 300 seconds is introduced above 10 km. The cloud physics includes only a Kessler type warm rain process. The turbulent mixing uses 1.5-order closure scheme based on the prediction of turbulent kinetic energy. The Coliolis force is not included. The whole calculation domain is 67.5 km × 33.9 km horizontally, and 14.1 km vertically. This domain is divided into eight subdomains, the size of which is 17.1 km × 17.1 km × 14.1 km. Each domain was calculated by one node.

The observed sounding data at Tateno (Figure 1) is given as a horizontally homogeneous basic state.

*Corresponding author address:
Akira NODA, Dynamic Marine Meteorology Group, Ocean Reserch Institute, University of Tokyo, 1-15-1, Minamidai, Nakano, Tokyo, 164-8639, Japan.
e-mail: noda@ori.u-tokyo.ac.jp

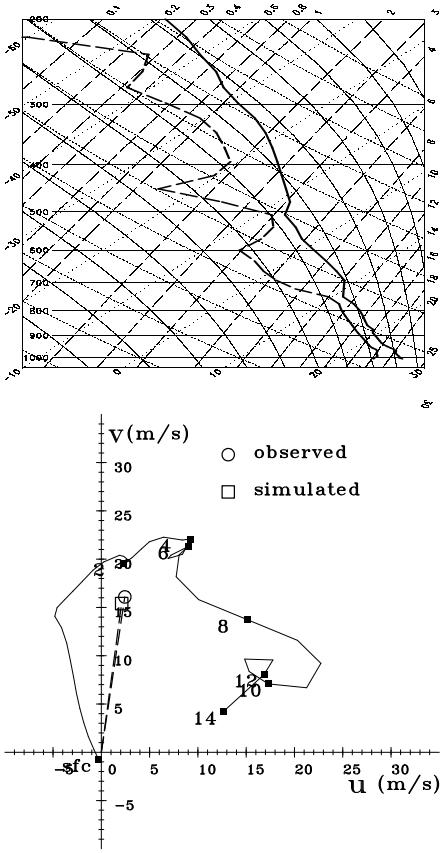

Figure 1: Upper-air sounding taken at Tateno at 2100 JST on 19 September 1990 used as a horizontally uniform basic state. (Upper) Skew T–log p diagram. The solid line shows temperature, and the dashed line dew-point temperature. (Lower) Wind hodograph. The integers by the solid square show the height in km. Observed and simulated storm motion are drawn by the open circle and open square, respectively.

In order to start a convection, a thermal bubble is placed at 1.5 km AGL at the horizontal center of the calculation domain. The maximum temperature anomaly of the bubble is 4 K. In order to keep the storm near the center of the calculation domain, the model coordinate system is translated by 2.0 ms^{-1}eastward and 16.0 ms^{-1}northward.

The simulation is performed for 160 minutes. Three dimensional data are stored every 10 minutes for later the analysis (except for the period between 6612 and 7812 seconds for which they are stored every 6 seconds for trajectory analysis).

3. OVERVIEW OF THE SIMULATED MINI-SUPERCELL

After 600 seconds from the start of the calculation, the direct influence of the initial bubble becomes unimportant, and the storm evolves in a manner governed by the environmental convective available potential energy, and the wind shear. As time elapses, a rain water pattern elongates in the north-south direction. An MC is formed at the southern end of the rain water pattern in agreement with the observation (Suzuki et al., 2000).

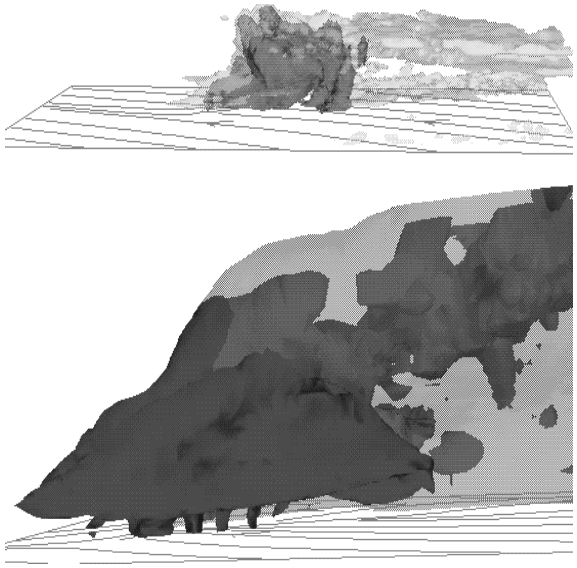

Figure 2: Three-dimensional views of the simulated supercell at 7812 seconds. (Upper) A total view of the simulated supercell. A part of the calculation domain of 67.5 km × 33.9 km × 14.1 km is shown. A cloud top is about 9.5 km. The near right corner is the northeast and the left corner the southeast. The light and dark shade show isosurfaces of 0.1 g/kg cloud water 1 g/kg rain water, respectively. Streamlines near the ground is also depicted. (Lower) Close-up view near the MC/TV at the left-side tip of the storm. Only the part of the domain (9.5 km × 7.1 km × 3.2 km) is shown. The light and dark shade now indicate isosurfaces of 1 g/kg rain water and 0.01 s^{-1}vertical vorticity, respectively. The thick vortex column is the TV discussed in the text.

After the vertical vorticity near the ground attained its first peak at around 3000 seconds, the supercell continues to maintain the similar magnitude of the vertical vorticity. The outflow spreading low-level from the storm meets the inflow, and a strong convergence region called a gust front is formed.

Around 7774 seconds, the vertical vorticity near the ground starts to increase rapidly. By 7812 seconds, its peak value exceeds 0.13 s^{-1}, a TV intensifies. Three-dimensional view of the whole storm and its close-up view near the TV at 7812 seconds are provided in Figure 2. The dimensions of the simulated supercell are small in agreement with the observation (Suzuki et al., 2000): The east-west width and north-south of the rain water pattern are about 5 km and 20 km, respectively, and the height of the anvil is at most 9.5 km. The MC defined by the region of an updraft with vertical vorticity larger than 10^{-2} s^{-1}has a north-south elongated structure with a horizontal length of 3 km, and occupies between 0.5 km and 1.5 km AGL. Below 500 m AGL at the southern end of the MC, a vertical column of high vorticity corresponding to the TV is seen. Its diameter is about 200 m. After attaining a peak of the vertical vorticity, it decays very quickly to 0.08 s^{-1}in 48 seconds. However, the storm as a whole continues to keep its overall organized structure and strength throughout the whole calculation.

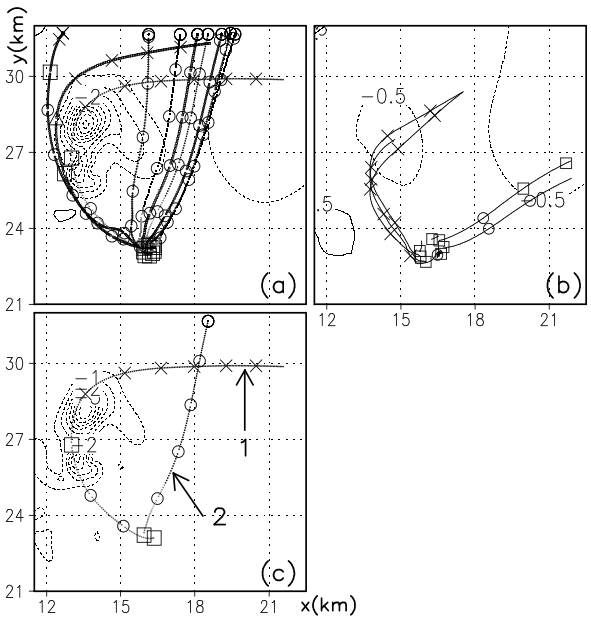

Figure 3: Horizontal cross section of decomposed pressure fields at 512 m AGL, at 7200 seconds. The contour lines are drawn for every 0.5 $\times 10^{-4}$. (a) Total pressure field and 20 minutes backward trajectories of air parcels placed around the TV (x=16, y=23) at 125 m AGL, at 7812 seconds. (b) Buoyancy pressure and vortex-lines passing near the TV, (c) Dynamic pressure and the trajectory for Parcel 1 and Parcel 2. Marks on the trajectories (vortex-lines) are drawn every 2 min (2 km) and denote the height: circle $\leq$ 100m $\leq$ square $\leq$ 200m $\leq$ triangle $\leq$ 300m $\leq$ cross.

4. ANALYSIS

In order to understand the mechanism to organize an airflow structure near the TV, backward trajectories of air parcels around the TV was calculated based on the three dimensional wind data stored every 6 seconds. The procedure to calculate the backward trajectories is as follows: Firstly, velocity vector of an air parcel is calculated by interpolating from eight adjacent grid points around it. Secondly, a location of the air parcel 6 seconds before is calculated from the interpolated velocity vector. Thirdly, this procedure is repeated 200 times to obtain a backward trajectories for 20 minutes.

Figure 3(a) depicts 20 minutes backward trajectories of 10 tracer parcels placed around the TV at 125 m AGL at 7812 seconds. It is seen that the trajectories coming into the TV consists of two major paths: One originates from about 600 m AGL to the northeast of the TV and descends to the low-level in its west while rotating cyclonically. The other originates near the surface to the north of the TV, and flows straightly southward into the TV. Hereafter, these two categories of trajectories will be represented by Parcel 1 and Parcel 2, respectively. Figure 3(b) shows a snap shot of vortex-lines passing near the TV at the same time. Again, the vortex-lines reaching the TV consist of two categories similar to those for backward trajectories. Especially for the trajectories originating from the mid-levels and the vortex-lines reaching the mid-levels show a good correspondence, indicating that the vortex-lines are nearly streamwise and the vertical vorticity in the TV originates from the horizontal vorticity associated with the horizontal wind at the mid-levels.

In order to examine the mechanism to cause these trajectories, the perturbation pressure field is decomposed in a similar manner to Rotunno and Klemp (1982). By taking divergence of the momentum equations under the Boussinesq approximation, a Poisson equation for the pressure may be given as:

$$\Delta\pi = -\frac{2}{C_p\Theta}\left(\frac{\partial v}{\partial x}\frac{\partial u}{\partial y} + \frac{\partial u}{\partial z}\frac{\partial w}{\partial x} + \frac{\partial v}{\partial z}\frac{\partial w}{\partial y}\right) - \frac{1}{C_p\Theta}\left[\left(\frac{\partial u}{\partial x}\right)^2 + \left(\frac{\partial v}{\partial y}\right)^2 + \left(\frac{\partial w}{\partial z}\right)^2\right] - \frac{g}{C_p\Theta^2}\frac{\partial \theta'}{\partial z},$$

where π is the Exner function, C_p (=1004 $\mathrm{m^2 s^{-2} K^{-1}}$) the specific heat of dry air at constant pressure, and Θ (=300 K) standard potential temperature. Since the left hand side of the Poisson equation is linear, perturbation pressure field can be decomposed into dynamic pressure (π_d) that depends on the velocities and buoyancy pressure (π_b) that depends on buoyancy. In solving the Poisson equations, boundary conditions for π_d is such that the normal gradient vanishes for the lateral and vertical boundaries. For π_b, they are that the normal gradient vanishes for the lateral boundaries and the hydrostatic balances hold for the vertical boundaries. Although the sum of the decomposed pressure fields does not exactly coincide with the original field owing to the turbulent mixing and numerical errors in solving Poisson equations, the difference is small and is insignificant for the following discussions.

To examine the driving mechanism of the mid-level air into the TV, a momentum budget analysis along the trajectories is performed using the following equation;

$$\frac{d\boldsymbol{v}}{dt} = \underbrace{-C_p\Theta\boldsymbol{\nabla}\pi_\mathrm{d}}_{dynamic} \underbrace{-C_p\Theta\boldsymbol{\nabla}\pi_\mathrm{b} - g\frac{\rho'}{\bar{\rho(z)}}\boldsymbol{k}}_{buoyancy}, \quad (1)$$

where $\bar{\rho(z)}$ is the density of the basic-state atmosphere at the height of the air parcel. The first term on the right hand side will be called a dynamic PGF, while the sum of the second and third terms a buoyancy force. The velocity vector of the parcel has been interpolated from the grid point data in the same way for the trajectory calculation. Dynamic and buoyancy pressure force are similarly evaluated from grid point data around the parcel. An accuracy of this budget analysis has been confirmed by checking that the velocity change calculated from Eulerian velocities along the trajectories coincides with the integration of the right hand side (RHS) of equation (1). Figure 4(a) shows the time evolution of velocity and terms in the RHS of (1) for the Parcel 1. Decomposed pressure fields at 512 m AGL, at 7200 seconds, are also shown in Figure 3 to see its variation along the parcel paths. Due to westward momentum of the environmental wind at the mid-level, the parcel moves initially westward. With slight acceleration by buoyancy PGF (Figure 3b), the parcel is drawn into the storm. As it moves closer to the main updraft, it starts to be affected by the dynamic PGF.

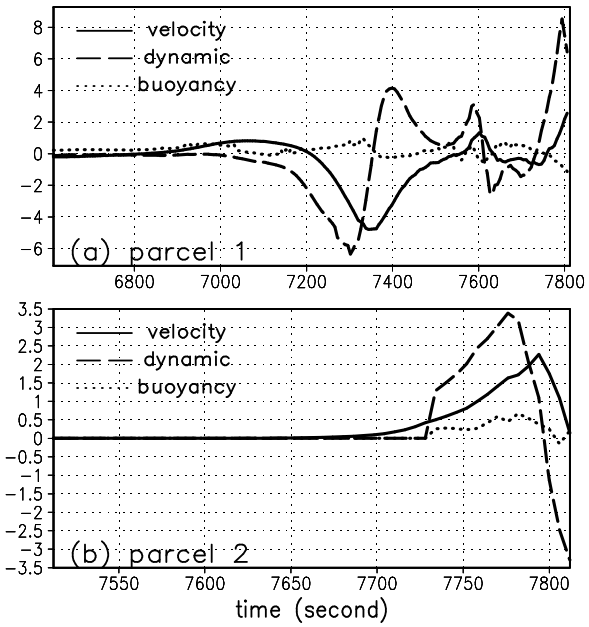

Figure 4: Time-evolution of vertical velocity, dynamic PGF and buoyancy force for (a) Parcel 1 and (b) Parcel 2. The solid lines show velocity (m/s), the dashed, dynamic pressure force (10^{-2} m s^{-2}), the dotted, buoyancy force (10^{-2} m s^{-2}). Only the results for the last 300 seconds are plotted for Parcel 2 since all of the values remain nearly zero before this period.

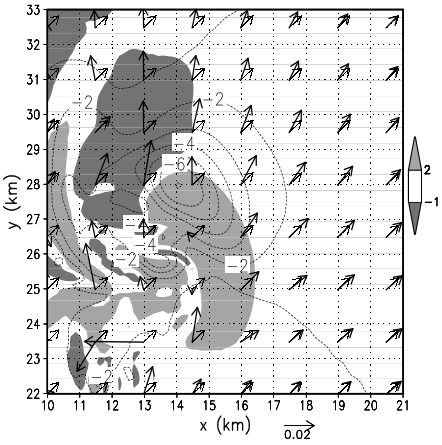

Figure 5: Horizontal cross section of the Exner function, vertical velocity and shear vectors at 1 km AGL, at 7200 seconds. The contour lines with an interval of 10^{-4} show the Exner function. Lightly shaded region shows updraft greater than 2 m/s, and darkly shaded region downdraft less than -1 m/s. Thick arrows show the shear vector field ($\frac{\partial u}{\partial z}, \frac{\partial v}{\partial z}$) for the total wind, while thin arrows that for the basic-state wind.

It works on the parcel as a centripetal force during its descent to the ground: The parcel rotates around the region of the maximum pressure deficit cyclonically. The parcel continues to be accelerated downward to the height of 300 m, where the pressure deficit is largest. After passing through this level, the dynamic PGF starts to decelerate the downward motion. Then, the low pressure associated with the TV (since it occurs in low-level, it is not seen in the level of 512 m indicated in Figure 3) draws the parcel into the TV. As it approaches the TV, the parcel starts to be lifted due to an upward acceleration caused by the mid-level shear and the strong convergence relating to the gust front. Although the path represented by parcel 1 is one of the important source of air flowing into the TV, the entrance from the mid-level to this path could be a narrow hole.

In order to acquire some idea about the size of the entrance hole, several tracer parcels are placed at the mid-level within 50 m from the air parcel that eventually reaches the TV near the ground, and their forward trajectories are calculated from 6612 to 7812 seconds. The result shows that most of trajectories of the tracer parcels deviate from the path of the original air parcel during the descent, and eventually diverge near the ground. To understand the downdraft furthermore, also performed is the similar momentum budget analysis along trajectories put on the storm-scale downdraft region near the ground (e.g., the area given by x=11-14 km and y=21-32 km in Figure 5) at about 500 m interval.

The result of the analysis shows that the dynamic PGF contributes to more than two thirds of the intensification of the downdraft.

A momentum budget of Parcel 2 is also shown in Figure 4(b). Initially, it is advected southward by the ambient northerly wind. As it approaches the storm center, it is accelerated southward by dynamic PGF. Storm-scale buoyancy force also contributes to westward acceleration. Eventually, rotationally-induced pressure depression draws it into the TV. As it approaches to the TV, it is first lifted by dynamic PGF, and then is decelerated by the rotationally-induced pressure gradient due to the lower-level rotation.

According to the theory by the interaction between the environmental shear and the storm updraft (Rotunno and Klemp, 1982), not only a low pressure in the downshear side of the updraft but also a high pressure should be generated in its upshear side. Such high pressure, however, is not evident in the simulated supercell. This may be explained as follows: The downshear side at the height of 512 m corresponds to upwind, so that the uniform environmental vertical wind shear remains without modification even after the storm evolution, and it produces the expected same sign of pressure perturbation. On the other hand, the upshear side is located downwind, where environmental wind is much more disturbed. As a result, the downshear side of low pressure dominates. The shear vectors of the basic state and of the total velocity field at 7200 seconds shown in Figure 5, in fact, confirms the above argument. Although the shear vector field is disturbed by the storm, the upwind side (northwest to northeast) relative to the updraft region (x=15, y=27) comparatively maintains the initial shear vectors. In contrast, that in the downwind side varies irregularly. As a result, perturbation pressure in the upshear side becomes less significant.

5. SUMMARY AND DISCUSSIONS

The structure of vortex-lines and airflows near the

TV of a mini-supercell which occurred over Kanto plain in Japan on 19 September 1990 are examined using a numerical simulation with a horizontal resolution of 150 m.

Airflows into the TV are found to consist of two major paths: One originates from about 600 m AGL to the northeast of the TV and descends to the low-levels in its west while rotating cyclonically. The other originates near the ground to the north of the TV and flows straightly southward into the TV. Vortex-lines which come into the TV show a close resemblance to trajectories that belong to the former path. It indicates that the mid-level environmental vorticity plays a significant role in generating the vertical vorticity of the TV. A momentum budget analysis along the trajectories shows that the dynamic PGF is important to drive the parcels from the mid-level to the TV near the ground.

In the previous studies, the generation and maintenance of the storm-scale downdraft in the supercell has been generally supposed to be a result of the negative buoyancy due to loading of hydrometeors and their evaporative cooling. In terms of the dynamic effect, Klemp and Rotunno (1983) suggested that the existence of the small-scale downdraft induced by low-level rotation. In this study, however, it has been clarified that the dynamic PGF relating to the interaction between an updraft and vertical wind shear (Rotunno and Klemp, 1982) plays an important role not only in the formation of the storm-scale updraft but also of the storm-scale downdraft originating from mid-level as illustrated in Browning (1964)'s conceptual model. Although the airflow structure in the supercell is relatively well-understood, why it can organize itself into such an efficient structure to last for several hours has not been completely understood. Present study suggests that to understand the mechanism of the downdraft could be another key factor to clarify the mechanism of its longevity.

The fact that a meso-low appears in the northeast gradient of the main updraft has been known both from observational and numerical studies (Charba and Sasaki, 1971; Weisman and Klemp, 1984; Wicker and Wilhelmson, 1995), which is generated by an interaction between the main updraft and vertical wind shear (Rotunno and Klemp, 1982). A majority of the veering wind shear environment, in which the shear vector varies from northwestward in the low-level to northeastward in the mid-level. For wind hodograph, the northwest to northeast side of the updraft corresponds to a downshear side as well as to upwind relative to the storm motion. Since environmental shear vector remains relatively undisturbed by the storm in the upwind side, the low pressure in the downshear side is more pronounced than the high pressure in the upshear side. One of the advantages for the shear-induced downdraft is that it develops in the downshear side of the main updraft and does not interfere with the main updraft. In this sense, the shear-induced downdraft due to strong veering low-level shear is important for the formation of a supercell. This mechanism to drive a downdraft dynamically is considered to apply not only for the supercell but also for other convections which occur in an environment with a strong vertical wind shear.

The effects of dynamic pressure demonstrated for the mini-supercell in this paper might be more pronounced than those for the classic supercell since the mini-supercell environment has a stronger low-level wind shear. Furthermore, the environment for a mini-supercell is more humid than that for a classic supercell, so that the evaporative cooling is less effective in the former. A similar momentum budget study on a classic supercell is being performed and the comparison of the results with the present study will be reported elsewhere.

ACKNOWLEDGMENTS

The present work is partly supported by Grant-in-Aids for Scientific Research on Priority Areas (B) No. 12125201, the Ministry of Education, Culture, Sports, Science, and Technology.

This simulation was made using the Advanced Regional Prediction System(ARPS) developed by the Center for Analysis and Prediction of Storms (CAPS), University of Oklahoma. CAPS is supported by the National Science Foundation and the Federal Aviation Administration through combined grant ATM92-20009.

REFERENCES

Browning, K. A., 1964: Airflow and precipitation trajectories within severe local storms which travel to the right of the winds. *J. Atmos. Sci.*, **21**, 634-639.

Burgess, D. W., R. A. Brown, L. R. Lemon, and C. R. Safford, 1977: Evolution of a tornadic thunderstorm. Preprints, *10th Conf. on Severe Local Storms*, Nebraska, Amer. Meteor. Soc., 84-89.

Charba., J., and Y. Sasaki, 1971: Structure and movement of the severe thunderstorms of 3 April 1964 as revealed from radar and surface mesonetwork data analysis. *J. Meteor. Soc. Japan*, **49**, 191-214.

Klemp, J. B., and R. B. Wilhelmson, and P. S. Ray, 1981: Observed and numerically simulated structure of a mature supercell thunderstorm. *J. Atmos. Sci.*, **38**, 1558-1580.

———, and R. Rotunno, 1983: A study of the tornadic region within a supercell thunderstorm. *J. Atmos. Sci.*, **40**, 359-377.

McCaul, E. W., Jr, 1991: Buoyancy and shear characteristics of hurricane-tornado environments. *Mon. Wea. Rev.*, **119**, 1954-1978.

———, and M. L. Weisman, 1996: Simulations of shallow supercell storms in landfalling hurricane environments. *Mon. Wea. Rev.*, **124**, 408-429.

Niino, H., and A. Noda, 2000: Numerical simulation of a mini-supercell over Kanto plain on 19 September 1990. Preprints, *20th Conf. on Severe Local Storms*, Orland, Florida, Amer. Meteor. Soc., 607-610.

Noda, A., 2000: The evolution of low-level mesocyclone in a mini supercell. Master thesis, University of Tokyo, 61 pp (in Japanese).

Novlan, D. J., and W. M. Gray, 1974: Hurricane-spawned tornadoes. *Mon. Wea. Rev.*, **102**, 476-488.

Rotunno, R., and J. B. Klemp, 1982: The influence of the shear-induced pressure gradient on thunderstorm motion. *Mon. Wea. Rev.*, **110**, 136-151.

Suzuki, O., H. Niino, H. Ohno, and H. Nirasawa, 2000: Tornado-producing mini supercells associated with typhoon 9019. *Mon. Wea. Rev.*, **128**, 1868-1882.

Weisman, M. L., and J. B. Klemp, 1984: The structure and classification of numerically simulated convective storms in directionally varying wind shears. *Mon. Wea. Rev.*, **112**, 2479-2498.

Wicker, L. J., and R. B. Wilhelmson, 1995: Simulation and analysis of tornado development and decay within a three dimensional supercell thunderstorm. *J. Atmos. Sci.*, **52**, 2675-2703.

Xue, M., K. K. Droegemeier, V. Wong, A. Shapiro, and K. Brewster, 1995: *ARPS Version 4.0 User's Guide*. The Center for Analysis and Prediction of Storms, University of Oklahoma, 380 pp.